A 36-Pulse Diode-Bridge Rectifier Using Dual Passive Harmonic Reduction Methods at DC Link

Lei Gao, Xiaona Xu, Zhongcheng Man, and Junyuan Lee

***Abstract*—In order to simultaneously reduce the harmonics of input line current and ripple of load voltage in multipulse diode-bridge rectifier, this paper proposes a 36-pulse rectifier using dual passive harmonic reduction methods at dc link. The proposed rectifier combines a 12-pulse rectifier and a multiwinding interphase reactor (IPR). The primary winding of the multiwinding IPR and two diodes constitute the double-tapped IPR, which is named as the first harmonic reduction method; the secondary winding of the multiwinding IPR and a single-phase diode-bridge rectifier formulate the second harmonic reduction method. When the multiwinding IPR is designed optimally, the pulse number of load voltage and step number of input line current can be increased from 12 to 24 by using the first method and from 24 to 36 by using the second method. The operation of the multiwinding IPR is analyzed, and the optimal turn ratio of the multiwinding IPR is obtained from the perspective of minimizing the total harmonic distortion of input line current. When the multiwinding IPR is designed optimally, both the pulse number of load voltage and step number of input line current are 36 per power supply cycle. Compared with the 12-pulse rectifier, in the proposed rectifier, the harmonics of input line current and ripple of load voltage are reduced significantly. The proposed rectifier is simpler and easier to realize than other methods. Some simulation and experiments are carried out to validate the theoretical analysis.**

***Index Terms*—Double-tapped interphase reactor (IPR), multipulse rectifier, multiwinding IPR, passive harmonic reduction, single-phase diode-bridge rectifier.**

I. Introduction

MULTIPULSE diode-bridge rectifier is the most popular rectifier in high power rectification system, such as ship propulsion system, aircraft power converter system, and long-range rocket launcher power supply system [1]–[3]. In these applications, multipulse diode-bridge rectifier is the interface between the load and generator, and transmits most of power produced by the generator. The performance of the multipulse diode-bridge rectifier, especially its power quality, affects the

Manuscript received February 26, 2018; accepted May 3, 2018. Date of publication May 10, 2018; date of current version December 7, 2018. This work was supported in part by the National Natural Foundation of China under Grant 51777042, in part by the China Postdoctoral Science Foundation under Grant 2016M590281 and Grant 2017T100241, and in part by the Scientific Research Foundation of Harbin Institute of Technology at Weihai under Grant WH20160105. Recommended for publication by Associate Editor J. Clare. *(Corresponding author: Lei Gao.)*

The authors are with the School of Electrical Engineering and Automation, Harbin Institute of Technology, Harbin 150006, China (e-mail:

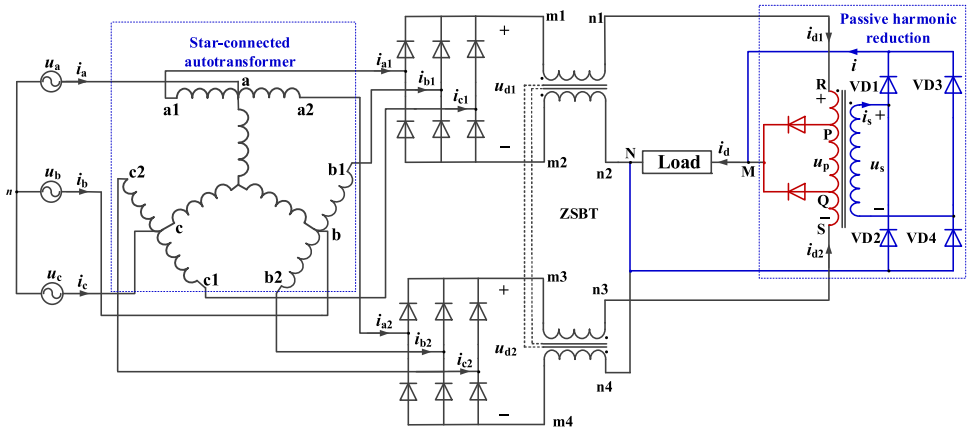

Fig. 1. Proposed multipulse rectifier using the dual passive harmonic reduction methods at dc link.

of the load voltage and step number of the input line current are 24 under the ideal condition [18], [20]. In this method, both the pulse number of the load voltage and the step number of the input line current are determined by the tap number of IPR and the number of three-phase diode-bridge rectifiers. In this method, when tap number of IPR is greater than two, the thyristors are used, and the control system becomes more and more complicated along with the increase of tap number of IPR [21], [22].

From the aforementioned analysis, the first method and the third method can simultaneously increase the pulse number of the load voltage and the step number of the input line current, and the second method can only reduce the harmonics in the input line current; in order to obtain higher pulse number and step number, more complicated winding configuration of phase-shifting transformer is a necessity in the first method, and more complicated control system is needed in the third method. Therefore, in order to improve the pulse number of load voltage and step number of input line current, using the passive auxiliary circuit at dc link is preferred.

In this paper, a 36-pulse diode-bridge rectifier using dual passive harmonic reduction methods at dc link is proposed. In the proposed rectifier, a multiwinding IPR is used, and its primary winding and two diodes constitute the conventional double-tapped IPR, which is the first harmonic reduction method; its secondary winding and a single-phase diode-bridge rectifier formulate the second harmonic reduction method. Because only the diodes are used in the dual passive harmonic reduction methods, the proposed rectifier is simple and easy to realize. More importantly, the dual passive harmonic methods can simultaneously increase the pulse number of the load voltage and step number of the input line current.

II. Topology and Mandatory Conditions of the Proposed Methods

Fig. 1 shows the proposed 36-pulse rectifier using the dual passive harmonic reduction methods at dc link. In Fig. 1, a star-connected autotransformer is used to be the phase-shifting transformer. Attention should be aroused that the other autotransformers or isolated transformers are also suitable to be

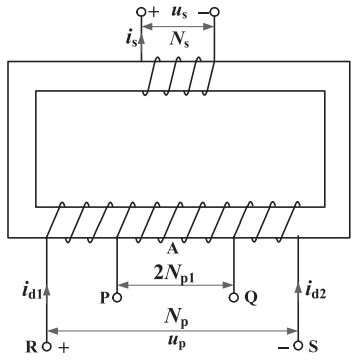

Fig. 2. Winding configuration of the multiwinding IPR.

the phase shifting transformer in the proposed rectifier. In the proposed rectifier, the IPR is replaced by a multiwinding IPR, and the primary winding of the multiwinding IPR and two common cathode-connected diodes constitute the well-known double-tapped IPR, which is named as the first passive harmonic reduction method; the secondary winding and a single-phase diode-bridge rectifier constitute the second method.

In Fig. 1, the input side (ac side) and output side (dc side) of the single-phase diode-bridge rectifier are connected with the secondary winding of the multiwinding IPR and the load, respectively. When the single-phase diode-bridge rectifier operates normally, the following mandatory condition should be met

$$|u_s|_{\max} \geq u_{\mathrm{da}\min} \tag{1}$$

where u_s is the voltage across the secondary winding of the multiwinding IPR, and $|u_s|_{\max}$ is the maximum of its absolute value; $u_{\mathrm{da\ min}}$ is the minimum of the load voltage u_{da}.

Fig. 2 shows the winding configuration of the multiwinding IPR, and in Fig. 2, two turn ratios are defined as

$$a_m = \frac{N_{p1}}{N_p}, \qquad m = \frac{N_s}{N_p} \tag{2}$$

where a_m and m are the turn ratio of the double-tapped IPR and the multiwinding IPR, respectively; N_{p1} is the turn number of winding AP or AQ, and N_p and N_s are the turn numbers of the primary winding and the secondary winding, respectively.

From Fig. 2 and (2), the relation between the voltages across the primary and secondary windings of the multiwinding IPR meets

$$m = \frac{u_s}{u_p}. \tag{3}$$

As discussed in [23], u_p is expressed as

$$u_p = \begin{cases} \dfrac{3\sqrt{2}E}{2+\sqrt{3}} \sin\left(\omega t - \pi - \dfrac{k\pi}{3}\right) & \omega t \in \left[\dfrac{k\pi}{3}, \dfrac{\pi}{12} + \dfrac{k\pi}{3}\right) \\ \dfrac{3\sqrt{2}E}{2+\sqrt{3}} \sin\left(\omega t - \dfrac{\pi}{6} - \dfrac{k\pi}{3}\right) & \omega t \in \left[\dfrac{\pi}{12} + \dfrac{k\pi}{3}, \dfrac{\pi}{4} + \dfrac{k\pi}{3}\right) \\ \dfrac{3\sqrt{2}E}{2+\sqrt{3}} \sin\left(\omega t + \pi - \dfrac{k\pi}{3}\right) & \omega t \in \left[\dfrac{\pi}{4} + \dfrac{k\pi}{3}, \dfrac{(k+1)\pi}{3}\right] \end{cases} \tag{4}$$

where *E* is the rms value of the input phase voltage. Thus, from (3) and (4), $|u_s|_{\max}$ is calculated as

$$|u_s|_{\max} = m|u_p|_{\max} = \frac{9\sqrt{3}-15}{2} mE. \tag{5}$$

As discussed in [23], after using the double-tapped IPR, the load voltage u_{da} is given by

$$u_{\mathrm{da}} = \begin{cases} \dfrac{3E}{\sqrt{2}} \left[\sin\left(\omega t + \dfrac{\pi}{2} - \dfrac{k\pi}{3}\right) + \dfrac{2a_m}{2+\sqrt{3}} \sin\left(\omega t - \dfrac{k\pi}{3}\right)\right] & \omega t \in \left[\dfrac{k\pi}{3}, \dfrac{\pi}{12} + \dfrac{k\pi}{3}\right) \\ \dfrac{3E}{\sqrt{2}} \left[\sin\left(\omega t + \dfrac{\pi}{3} - \dfrac{k\pi}{3}\right) - \dfrac{2a_m}{2+\sqrt{3}} \sin\left(\omega t - \dfrac{\pi}{6} - \dfrac{k\pi}{3}\right)\right] & \omega t \in \left[\dfrac{\pi}{12} + \dfrac{k\pi}{3}, \dfrac{\pi}{6} + \dfrac{k\pi}{3}\right) \\ \dfrac{3E}{\sqrt{2}} \left[\sin\left(\omega t + \dfrac{\pi}{3} - \dfrac{k\pi}{3}\right) + \dfrac{2a_m}{2+\sqrt{3}} \sin\left(\omega t - \dfrac{\pi}{6} - \dfrac{k\pi}{3}\right)\right] & \omega t \in \left[\dfrac{\pi}{6} + \dfrac{k\pi}{3}, \dfrac{\pi}{4} + \dfrac{k\pi}{3}\right) \\ \dfrac{3E}{\sqrt{2}} \left[\sin\left(\omega t + \dfrac{\pi}{6} - \dfrac{k\pi}{3}\right) + \dfrac{2a_m}{2+\sqrt{3}} \sin\left(\omega t + \dfrac{2\pi}{3} - \dfrac{k\pi}{3}\right)\right] & \omega t \in \left[\dfrac{\pi}{4} + \dfrac{k\pi}{3}, \dfrac{(k+1)\pi}{3}\right]. \end{cases} \tag{6}$$

From (6), $u_{\mathrm{da\,min}}$ is calculated as

$$u_{da\min} = 3\left(\frac{1+\sqrt{3}}{4} + \frac{3\sqrt{3}-5}{2} a_m\right) E. \tag{7}$$

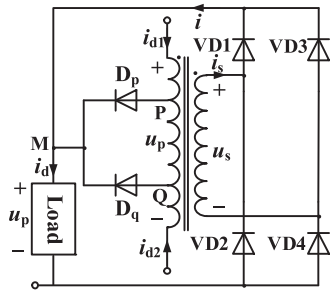

Fig. 3. Multiwinding IPR and its auxiliary circuit.

Substituting (5) and (7) into (1) yields

$$m \geq \frac{12+7\sqrt{3}}{6} + a_m. \tag{8}$$

In addition, from Fig. 2 and (2), the turn ratio a_m should meet

$$0 \leq a_m \leq 0.5. \tag{9}$$

When the two turn ratios meet (8) and (9), the single-phase diode-bridge rectifier can operate normally.

As discussed in [23], the turn ratio of the double-tapped IPR affects the pulse number of load voltage; in Fig. 1, because the output side of the single-phase diode-bridge rectifier connects with the load, the turn ratio of the multiwinding IPR also affects inevitably the pulse number of load voltage. Expressions (8) and (9) limit the ranges of the two turn ratios. In next section, the multiwinding IPR is designed optimally to obtain the THD minimum of the input line currents.

III. Optimal Design of the Multiwinding IPR

In this section, from the perspective of minimizing the THD of input line current, the multiwinding IPR is optimally designed.

A. Operation Modes of the Multiwinding IPR

Fig. 3 shows the multiwinding IPR and its auxiliary circuit. As discussed in this section [23], the double-tapped IPR has two operation modes: ①when $u_p > 0$, the diode D_p conducts, and the double-tapped IPR operates at mode P; ②when $u_p < 0$, the diode D_q conducts, and the double-tapped IPR operates at mode Q. According to the operation principle, the single-phase diode-bridge rectifier has three operation modes: ①when $|u_s| < u_d$, the diodes VD1, VD2, VD3, and VD4 are reverse-biased; ②when $u_s > u_d$, the diodes VD1 and VD4 conduct, and the diodes VD2 and VD3 are reverse-biased; ③when $-u_s > u_d$, the diodes VD2 and VD3 conduct, and the diodes VD1 and VD4 are reverse-biased. Therefore, the multiwinding IPR and its auxiliary circuit have six operation modes.

When the single-phase diode-bridge rectifier operates normally, its output voltage is equal to the load voltage

$$u_d(\phi) = |u_s(\phi)| = m\,|u_p(\phi)| \tag{10}$$

where ϕ is the initial conduct angle of the single-phase diode-bridge rectifier.

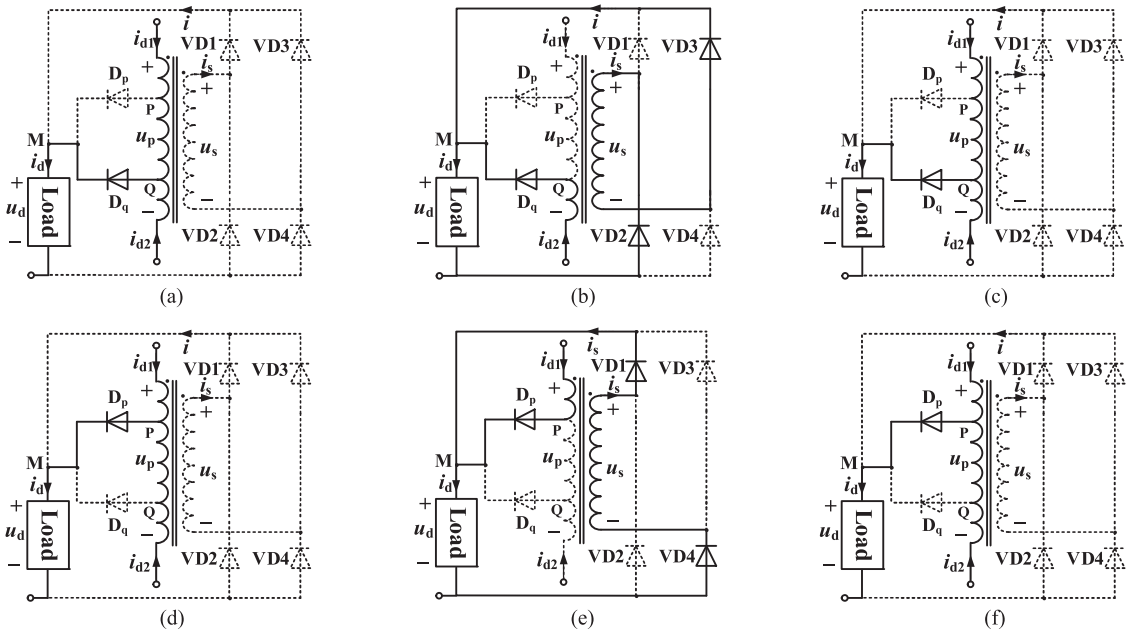

Fig. 4. Operation mode of the multi-winding IPR. (a) Mode I: $\omega t \in [0,\ \phi]$. (b) Mode II: $\omega t \in [\phi,\ \pi/6-\phi]$. (c) Mode III: $\omega t \in [\pi/6-\phi,\ \pi/6]$. (d) Mode IV: $\omega t \in [\pi/6,\ \pi/6+\phi]$. (e) Mode V: $\omega t \in [\pi/6+\phi,\ \pi/3-\phi]$. (f) Mode IV: $\omega t \in [\pi/6-\phi,\ \pi/6]$.

From (3) and (4), the period of the voltage $|u_s|$ is $\pi/6$. Therefore, the initial conduct angle ϕ meets

$$0 < \phi < \frac{\pi}{12}. \tag{11}$$

From (5), (6), and (10), ϕ is calculated as

$$\phi = \arctan\frac{2+\sqrt{3}}{2(m-a_m)}. \tag{12}$$

From (4) and (6), the periods of the voltages u_p, u_s, $|u_s|$, u_{da} are $\pi/3$, $\pi/3$, $\pi/6$ and $\pi/6$, respectively. Therefore, the operation modes can be analyzed in the interval $[0,\ \pi/3]$.

1) Mode I: $\omega t \in [0,\ \phi]$*:* In this interval, u_p is less than zero, and $|u_s|$ is less than u_d. Therefore, the diode D_q is forward-biased and turns on, the single-phase diode-bridge rectifier does not work, and the output current of the single-phase diode-bridge rectifier is equal to zero. Fig. 4(a) shows the operation mode.

From the ampere-turn balance principle and Kirchhoff's voltage law, the currents i_{d1}, i_{d2} and load voltage are calculated as

$$\begin{cases} i_{d1} = 0.5I_d - i_m \\ i_{d2} = 0.5I_d + i_m \\ u_d = 0.5(u_{d1} + u_{d2}) \end{cases} \tag{13}$$

where i_m is the circulating current and it is equal to $a_m I_d$.

2) Mode II: $\omega t \in [\phi,\ \pi/6-\phi]$*:* In this interval, u_p is less than zero, and $-u_s$ is greater than u_d. Therefore, the diodes D_q, VD2 and VD3 are forward-biased and turn on, and the diodes VD1 and VD4 are reverse-biased and turn off. Fig. 4(b) shows the operation mode.

From the ampere-turn balance principle and the operation principle of the single-phase diode-bridge rectifier, the currents i, i_{d1} and i_{d2} are calculated as

$$\begin{cases} i = \dfrac{1-2a_m}{2m+1-2a_m} I_d \\ i_{d2} = \dfrac{2m}{2m+1-2a_m} I_d, \text{ and } i_{d1} = 0. \end{cases} \tag{14}$$

From the Kirchhoff's voltage law, the relation among u_d, u_{d1}, u_{d2}, u_s, and u_p meets

$$\begin{cases} u_d = -u_s = u_{d2} + (0.5 - a_m)u_p \\ u_p = \dfrac{u_s}{m}, \text{ and } u_{d2} + u_p = u_{d1}. \end{cases} \tag{15}$$

Therefore,

$$\begin{cases} u_d = -u_s = \dfrac{2m}{2m+1-2a_m} u_{d2} \\ u_{d1} = \dfrac{2m-1-2a_m}{2m+1-2a_m} u_{d2} \\ u_p = -\dfrac{2}{2m+1-2a_m} u_{d2}. \end{cases} \tag{16}$$

3) Mode III: $\omega t \in [\pi/6-\phi,\ \pi/6]$*:* In this interval, u_p is less than zero, and $|u_s|$ is less than u_d, which is the same as that in the mode I.

4) Mode IV: $\omega t \in [\pi/6,\ \pi/6+\phi]$*:* In this interval, u_p is greater than zero, and $|u_s|$ is less than u_d. Therefore, the diodes D_p is forward-biased and turns on, and the single-phase diode-bridge rectifier does not work. Fig. 4(d) shows the operation mode. From the ampere-turn balance principle and Kirchhoff's voltage law, the currents i_{d1}, i_{d2} and load voltage are

calculated as

$$\begin{cases} i_{d1} = 0.5I_d + i_m \\ i_{d2} = 0.5I_d - i_m \\ u_d = 0.5(u_{d1} + u_{d2}). \end{cases} \tag{17}$$

5) Mode V: $\omega t \in [\pi/6 + \phi,\ \pi/3 - \phi]$*:* In this interval, u_p is greater than zero, and u_s is greater than u_d. Therefore, the diodes D_p, VD1 and VD4 are forward-biased and turn on, and the diodes VD2 and VD3 are reverse-biased and turn off. Fig. 4(e) shows the operation mode.

From the ampere-turn balance principle and the operation principle of the single-phase diode-bridge rectifier, the currents i, i_{d1} and i_{d2} are calculated as

$$\begin{cases} i = \dfrac{1 - 2a_m}{2m + 1 - 2a_m} I_d \\ i_{d1} = \dfrac{2m}{2m + 1 - 2a_m} I_d, \text{ and } i_{d2} = 0. \end{cases} \tag{18}$$

From the Kirchhoff's voltage law, the relation among u_d, u_{d1}, u_{d2}, u_s, and u_p meets

$$\begin{cases} u_d = u_s = u_{d1} - (0.5 - a_m)u_p \\ u_p = \dfrac{u_s}{m}, \text{ and } u_{d1} - u_p = u_{d2}. \end{cases} \tag{19}$$

Therefore,

$$\begin{cases} u_d = u_s = \dfrac{2m}{2m + 1 - 2a_m} u_{d1} \\ u_{d2} = \dfrac{2m - 1 - 2a_m}{2m + 1 - 2a_m} u_{d1} \\ u_p = \dfrac{2}{2m + 1 - 2a_m} u_{d1}. \end{cases} \tag{20}$$

6) Mode VI: $\omega t \in [\pi/6 - \phi,\ \pi/6]$*:* In this interval, u_p is greater than zero, and $|u_s|$ is less than u_d, which is the same as that in the mode IV

From the aforementioned analysis, the current i_{d1} through the primary winding of the multiwinding IPR is expressed as

$$i_{d1} = \begin{cases} (0.5 - a_m)I_d & \omega t \in \left[\dfrac{k\pi}{3}, \phi + \dfrac{k\pi}{3}\right] \\ 0 & \omega t \in \left[\phi + \dfrac{k\pi}{3}, \dfrac{\pi}{6} - \phi + \dfrac{k\pi}{3}\right) \\ (0.5 - a_m)I_d & \omega t \in \left[\dfrac{\pi}{6} - \phi + \dfrac{k\pi}{3}, \dfrac{\pi}{6} + \dfrac{k\pi}{3}\right) \\ (0.5 + a_m)I_d & \omega t \in \left[\dfrac{\pi}{6} + \dfrac{k\pi}{3}, \dfrac{\pi}{6} + \phi + \dfrac{k\pi}{3}\right) \\ \dfrac{2mI_d}{2m + 1 - 2a_m} & \omega t \in \left[\dfrac{\pi}{6} + \phi + \dfrac{k\pi}{3}, \dfrac{\pi}{3} - \phi + \dfrac{k\pi}{3}\right) \\ (0.5 + a_m)I_d & \omega t \in \left[\dfrac{\pi}{3} - \phi + \dfrac{k\pi}{3}, \dfrac{(k+1)\pi}{3}\right]. \end{cases} \tag{21}$$

The current i_{d2} lags behind i_{d1} $\pi/6$ electric degree.

B. Optimal Turn Ratio of the Multiwinding IPR

In part A of this section, the currents i_{d1} and i_{d2} are obtained by analyzing the operation of the multiwinding IPR. When i_{d1} and i_{d2} are known, the input line currents of the proposed rectifier can be calculated, and furthermore, the optimal turn ratios of the multiwinding IPR can be obtained by minimizing the THD of the input line current.

As discussed in [23], the input line currents are expressed as

$$\begin{cases} i_a = [S_{a1} + (2 - \sqrt{3})S_{b1}]i_{d1} + [S_{a2} + (2 - \sqrt{3})S_{c2}]i_{d2} \\ i_b = [S_{b1} + (2 - \sqrt{3})S_{c1}]i_{d1} + [S_{b2} + (2 - \sqrt{3})S_{a2}]i_{d2} \\ i_c = [S_{c1} + (2 - \sqrt{3})S_{a1}]i_{d1} + [S_{c2} + (2 - \sqrt{3})S_{b2}]i_{d2} \end{cases} \tag{22}$$

where S_{a1}, S_{b1}, S_{c1}, S_{a2}, S_{b2}, S_{c2} are the switching functions of the phase a1, b1, c1, a2, b2, c2, respectively.

To set phase **a** as an example, substituting (21) into (22), the Fourier series of the current i_a is calculated as

$$i_a = \sum_{n=1}^{\infty} \frac{2I_d}{n\pi} B_n \sin(n\omega t) \tag{23}$$

where B_n meets

$$\begin{aligned} B_n = 2\sin\frac{n\pi}{2} \Bigg\{ & 2(2 - \sqrt{3})a_m \sin\frac{n\pi}{3}\left(2\cos\frac{n\pi}{6} + \sqrt{3}\right) \\ & + \sin n\phi\left(\cos\frac{n\pi}{3} + \sqrt{3}\cos\frac{n\pi}{6} + 1\right) - 2(2 - \sqrt{3})a_m \\ & \times \left[\left(\sqrt{3}\sin\frac{n\pi}{3} + \sin\frac{n\pi}{6}\right)\cos n\phi + \sin\left(\frac{n\pi}{2} - n\phi\right)\right] \\ & + \frac{4m\sin\left(\frac{n\pi}{12} - n\phi\right)}{2m + 1 - 2a_m}\left(\frac{2\cos\frac{n\pi}{4}}{\sqrt{3}+1} + \frac{\cos\frac{5n\pi}{12}}{2+\sqrt{3}} + \cos\frac{n\pi}{12}\right)\Bigg\}. \end{aligned}$$

From (23), the rms value of the current i_a is calculated as

$$I_a = I_d\sqrt{6[1 + 4(7 - 4\sqrt{3})a_m^2]\frac{\phi}{\pi} + \frac{8(2-\sqrt{3})m^2}{(2m+1-2a_m)^2}\left(1 - \frac{12\phi}{\pi}\right)} \tag{24}$$

and the rms value of its fundamental is calculated as

$$I_a' = \frac{\sqrt{2}I_d}{\pi} B_1 \tag{25}$$

where $B_1 = \frac{12}{2+\sqrt{3}}[a_m(1 - \cos\phi) + \frac{m\cos\phi}{2m+1-2a_m}] + \frac{6(1-2a_m)\sin\phi}{2m+1-2a_m}$.

Define the THD of the input line current as

$$\mathrm{THD} = \frac{\sqrt{I_a^2 - I_a'^2}}{I'_a}. \tag{26}$$

The THD of input line current can be obtained by substituting (24) and (25) into (26). Fig. 5(a) shows the relation among the THD, a_m and m. In Fig. 5(a), when $a_m = 0.163$ and $m = 10.75$, the THD is minimal, and the minimum is 5.04%; from (17), when $a_m = 0.163$ and $m = 10.75$, $\phi = 10°$. When $a_m = 0.163$, Fig. 9(b) shows the relation between the THD and m; when $m = 10.75$, Fig. 5(c) shows the relation between the THD and a_m.

When $a_m = 0.163$ and $m = 10.75$, Fig. 6 shows the input line current and its spectrum. The input line current contains

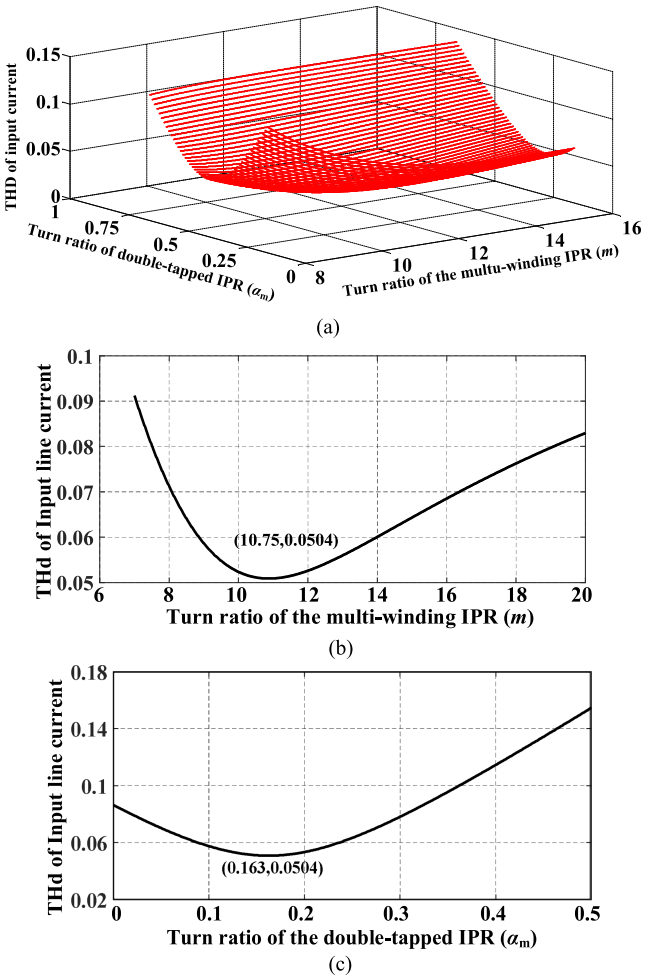

Fig. 5. Relation among the THD, a_m and m. (a) Global relation. (b) Relation between the THD and m when $a_m = 0.163$. (c) Relation between the THD and a_m when $m = 10.75$.

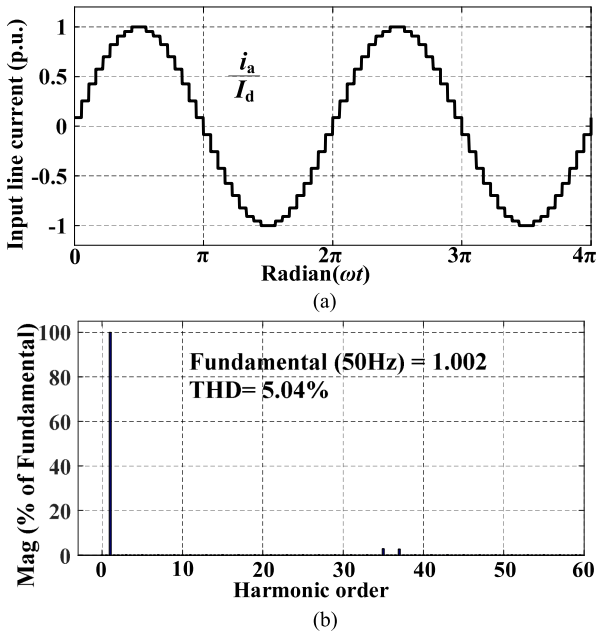

Fig. 6. Input line current and its spectrum under the optimal turn ratio. (a) Input line current. (b) Spectrum of the input line current.

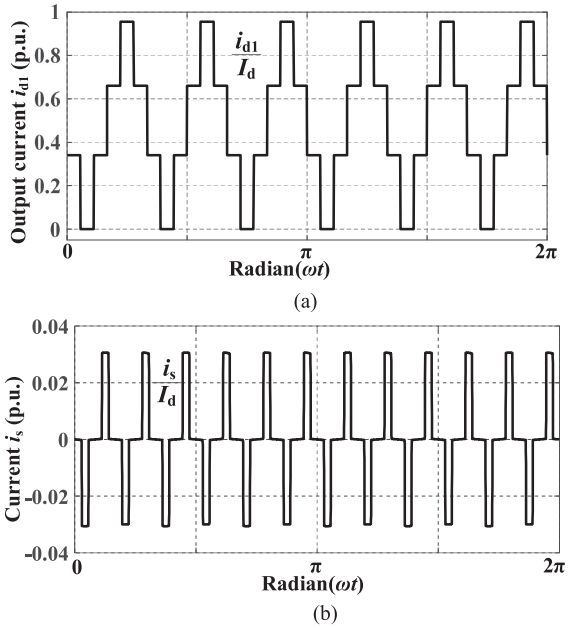

Fig. 7. Currents through the windings of the multiwinding IPR. (a) Current i_{d1}. (b) Current i_s.

36 steps with the equal width per power supply cycle, and its THD is about 5.04%; from Fig. 6(b), the lowest harmonic is 35 order. Therefore, from the waveform of the input line current, the proposed multipulse rectifier realizes the 36 pulse rectification.

When $a_m = 0.163$ and $m = 10.75$, Fig. 7 shows i_s and i_{d1}.

C. Load Voltage

From the analysis of the operation of the multiwinding IPR, the load voltage u_d is expressed as

$$u_d = \begin{cases} \dfrac{3E}{\sqrt{2}}\left[\sin\left(\omega t+\dfrac{\pi}{2}-\dfrac{k\pi}{6}\right)+\dfrac{2a_m}{2+\sqrt{3}}\sin\left(\omega t-\dfrac{k\pi}{6}\right)\right] \\ \qquad \omega t \in \left[\dfrac{k\pi}{6}, \dfrac{\pi}{18}+\dfrac{k\pi}{6}\right) \\ \dfrac{6m(\sqrt{3}-1)E}{2m+1-2a_m}\sin\left(\omega t+\dfrac{5\pi}{12}-\dfrac{k\pi}{6}\right) \\ \qquad \omega t \in \left[\dfrac{\pi}{18}+\dfrac{k\pi}{6}, \dfrac{\pi}{9}+\dfrac{k\pi}{6}\right) \\ \dfrac{3E}{\sqrt{2}}\left[\sin\left(\omega t+\dfrac{\pi}{3}-\dfrac{k\pi}{6}\right)-\dfrac{2a_m}{2+\sqrt{3}}\sin\left(\omega t-\dfrac{\pi}{6}-\dfrac{k\pi}{6}\right)\right] \\ \qquad \omega t \in \left[\dfrac{\pi}{9}+\dfrac{k\pi}{6}, \dfrac{(k+1)\pi}{6}\right]. \end{cases} \tag{27}$$

When $a_m = 0.163$, $m = 10.75$, the load voltage $u_{\rm d}$ can be illustrated, as shown in Fig. 8. The load voltage has 36 pulses with equal width per power supply cycle. Therefore, from the waveform of load voltage, the proposed multipulse rectifier also realizes 36-pulse rectification.

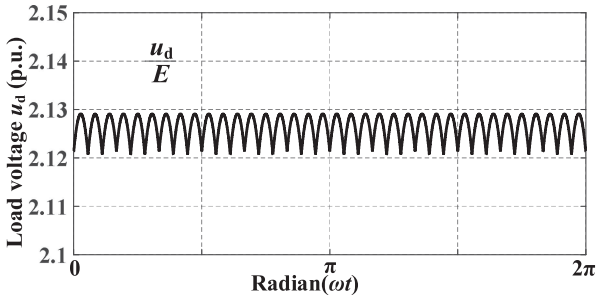

Fig. 8. Theoretical waveform of load voltage under the optimal turn ratio.

From (27), the maximum, minimum, and average value of the load voltage are calculated as

$$\begin{cases} u_{\mathrm{dmax}} = 2.129E \\ u_{\mathrm{dmin}} = 2.121E \\ u_{\mathrm{dav}} = 2.1264E. \end{cases} \tag{28}$$

Define the ripple coefficient as

$$K = \frac{u_{\mathrm{dmax}} - u_{\mathrm{dmin}}}{2u_{\mathrm{dav}}}. \tag{29}$$

Substituting (28) into (29), the ripple coefficient of load voltage is calculated to be 1.88×10^{-3}, which is far less than that of the 12-pulse rectifier and 24-pulse rectifier in [20].

D. Discussion About kVA Ratings of the Multiwinding IPR

As discussed in [23], in the 12-pulse rectifier, the kVA rating of the IPR accounts 2.03% of the load power. In this part, the kVA rating of the multiwinding IPR is calculated when the dual passive harmonic reduction methods are used.

From the operation modes of the multiwinding IPR, the rms value of the voltage across its primary winding is calculated as

$$U_p = 3\sqrt{2}(2-\sqrt{3})\sqrt{\frac{1}{2} - \frac{3}{2\pi}}E \approx 0.17E. \tag{30}$$

From Fig. 2, the primary winding of the multiwinding IPR comprises three little windings (winding RP, winding PQ, and winding QS). The currents through the winding RP and winding QS are equal to I_{d1} and I_{d2}, and their rms values are calculated as

$$\begin{aligned} I_{d1} = I_{d2} &= I_d\sqrt{a_m^2 \times \frac{2}{3} + \left(\frac{2m}{2m+1}\right)^2 \times \frac{1}{6} + \frac{1}{6}} \\ &= 0.5796 I_d. \end{aligned} \tag{31}$$

From the operation mode of the multiwinding IPR, the current through the winding PQ is expressed as

$$i_{\mathrm{PQ}} = \begin{cases} \dfrac{I_d}{2} - a_m I_d & \omega t \in \left[\dfrac{\pi}{3}k, \dfrac{\pi}{18} + \dfrac{\pi}{3}k\right) \\ 0 & \omega t \in \left[\dfrac{\pi}{18} + \dfrac{\pi}{3}k, \dfrac{\pi}{9} + \dfrac{\pi}{3}k\right) \\ \dfrac{I_d}{2} - a_m I_d & \omega t \in \left[\dfrac{\pi}{9} + \dfrac{\pi}{3}k, \dfrac{\pi}{6} + \dfrac{\pi}{3}k\right) \\ -\dfrac{I_d}{2} + a_m I_d & \omega t \in \left[\dfrac{\pi}{6} + \dfrac{\pi}{3}k, \dfrac{2\pi}{9} + \dfrac{\pi}{3}k\right) \\ 0 & \omega t \in \left[\dfrac{2\pi}{9} + \dfrac{\pi}{3}k, \dfrac{5\pi}{18} + \dfrac{\pi}{3}k\right) \\ -\dfrac{I_d}{2} + a_m I_d & \omega t \in \left[\dfrac{5\pi}{18} + \dfrac{\pi}{3}k, \dfrac{\pi}{3}(k+1)\right] \end{cases} \quad k = 0, 1, 2 \ldots \tag{32}$$

and its rms value is calculated as

$$I_{\mathrm{PQ}} = \sqrt{\frac{2}{3}}\left(\frac{1}{2} - a_m\right) I_d = 0.2776 I_d. \tag{33}$$

From (3) and (30), under the optimal turn ratio condition, the rms value of the voltage across the secondary winding is calculated as

$$U_s = mU_p \approx 10.75 \times 0.17E = 1.8275E. \tag{34}$$

From the operation modes of the multiwinding IPR, the rms value of the current through the secondary winding of the multiwinding IPR is calculated as

$$I_s = \sqrt{\frac{1}{3}}\frac{1-2a_m}{2m+1-2a_m} I_d = 0.01755 I_d. \tag{35}$$

Therefore, the kVA rating is calculated as

$$\begin{aligned} S_{\mathrm{IPR}} = \frac{1}{2} \times \Bigg[& 2 \times \left(\frac{1}{2} - a_m\right) \times 0.17 \\ & \times \sqrt{\frac{2}{3}a_m^2 + \frac{1}{6}\left(\frac{2m}{2m\ +\ 1}\right)^2 + \frac{1}{6}} + 2a_m 0.17\sqrt{\frac{2}{3}} \\ & \times \left(\frac{1}{2} - a_m\right) + 1.8275\sqrt{\frac{1}{3}}\frac{1-2a_m}{2m+1-2a_m}\Bigg] \\ I_d = 0.057 E I_d &= 2.68\% U_d I_d. \end{aligned} \tag{36}$$

The kVA rating of the multiwinding IPR accounts for 2.68% of the load power. Compared with the IPR, the multiwinding IPR has a secondary winding. In addition, the modulation effect of the dual methods has changed the currents through the primary winding of the IPR. Therefore, the kVA rating of the multiwinding IPR is greater than that of the IPR.

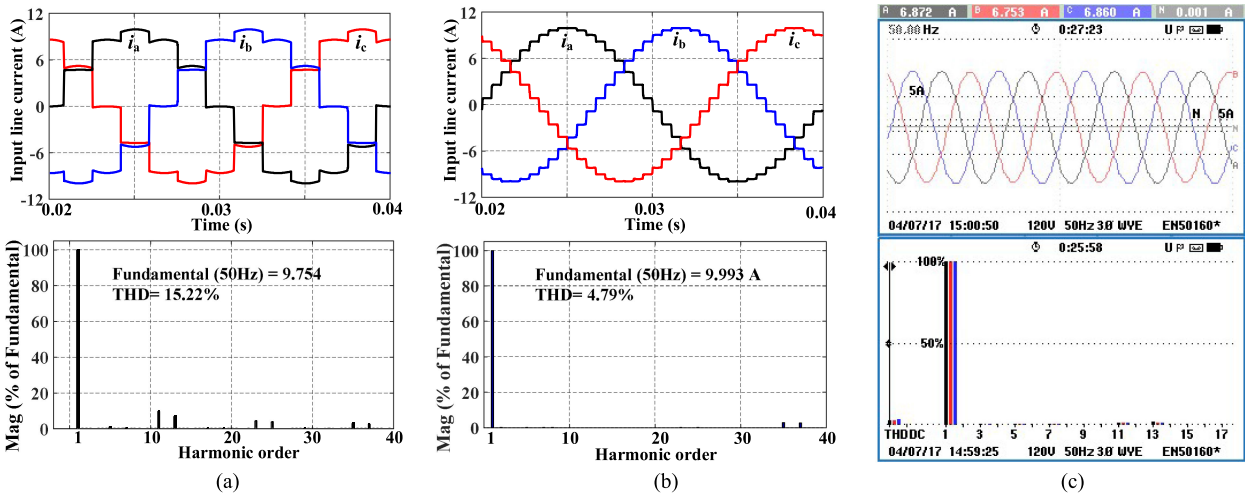

Fig. 9. Input line currents and their spectrums. (a) Simulation results of the 12-pulse rectifier. (b) Simulation results of the proposed multipulse rectifier. (c) Experimental results of the proposed multipulse rectifier.

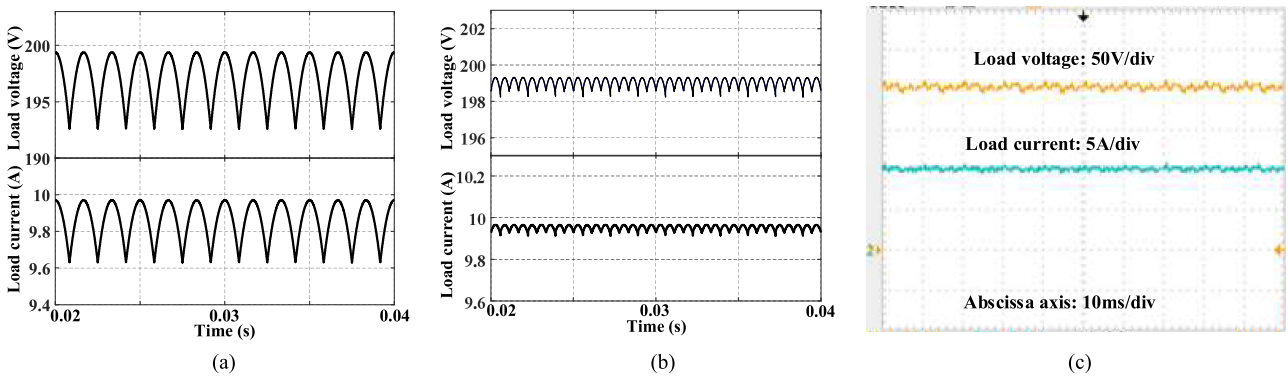

Fig. 10. Load voltage and load current. (a) Simulation results of the 12-pulse rectifier. (b) Simulation results of the proposed multipulse rectifier. (c) Experimental results of the proposed multipulse rectifier.

IV. Experimental Validation

From the theoretical analysis in Section III, the proposed rectifier has good performance in reducing harmonics of input line currents and ripple of load voltage. In order to validate the aforementioned theoretical analysis, a 36-pulse rectifier using the dual passive harmonic reduction methods is designed. Some simulation and experiments are carried out, and the simulation and experimental conditions are listed as follows:

1) The rms value of input phase voltage is 95 V.
2) Load power is 2 kW.
3) Load resistance is 20 Ω.
4) $N_s = 947, N_p = 88, N_{p1} = 14$.

Fig. 9(a) shows the input line currents and their spectrums in the 12-pulse rectifier, and Fig. 9(b) and (c) shows the corresponding simulation and experimental results in the proposed multipulse rectifier, respectively. In the 12-pulse rectifier, the THD of input line current is about 15%, and the lowest harmonic is 11 order; in the proposed multipulse rectifier, the simulation and experimental value of the THD are about 4.8% and 3.1%, respectively, and the lowest harmonic is 35 order. From Fig. 9(b) and (c), the input line currents are approximately sinusoidal, and the experimental value of THD is less than the theoretical value because of the effect of leakage inductance of phase-shifting transformer. Compared with the input line currents of the 12-pulse rectifier, the harmonics in the proposed rectifier are reduced significantly.

Fig. 10(a) shows the load voltage and load current in the 12-pulse rectifier, and Fig. 10(b) and (c) shows the corresponding simulation and experimental results in the proposed multipulse rectifier, respectively. In the 12-pulse rectifier, the load voltage has 12 pulses per power supply cycle; in the proposed multipulse rectifier, the load voltage has 36 pulses per power supply cycle. From Fig. 10(c), the load voltage and load current are approximately constant, which indicates that their ripple coefficients are very small. In addition, when simulating, the inductance of the multiwinding IPR is set to be very small, but when experimenting, the inductance cannot be ignored. Therefore, the experimental results of load voltage and load current are smoother than that of the simulating results.

Fig. 11(a) shows the output currents and output voltages of the two three-phase diode-bridge rectifiers in the 12-pulse rectifier, and Fig. 11(b) and (c) shows the corresponding simulation

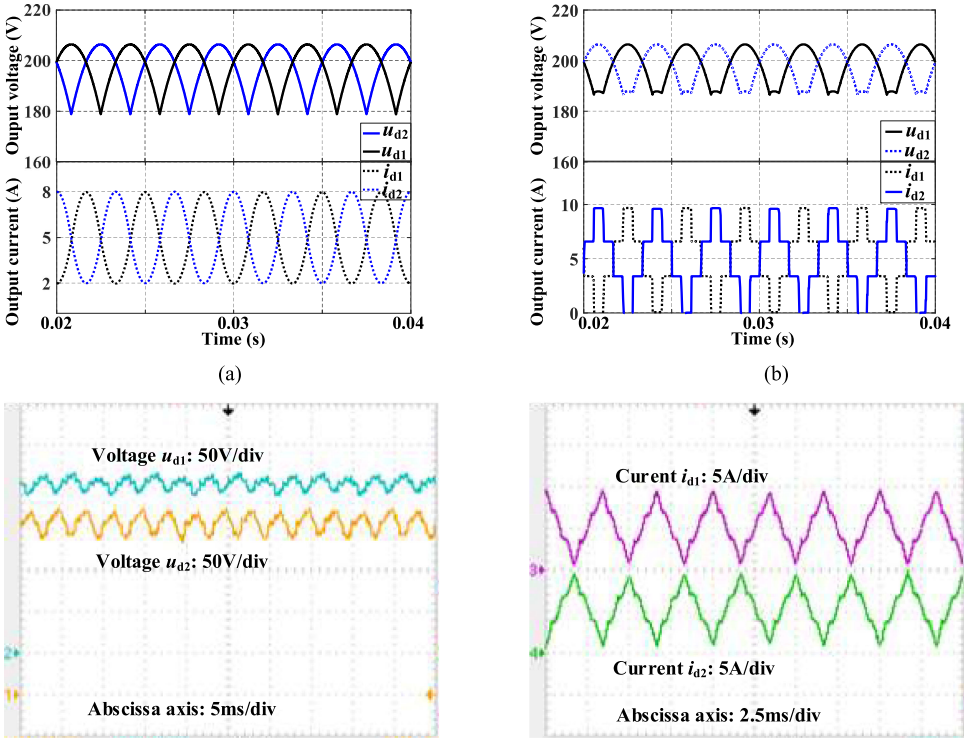

Fig. 11. Output currents and output voltages of the two three-phase diode-bridge rectifiers. (a) Simulation result of the 12-pulse rectifier. (b) Simulation result of the proposed multi-pulse rectifier. (c) Experimental result of the proposed multi-pulse rectifier.

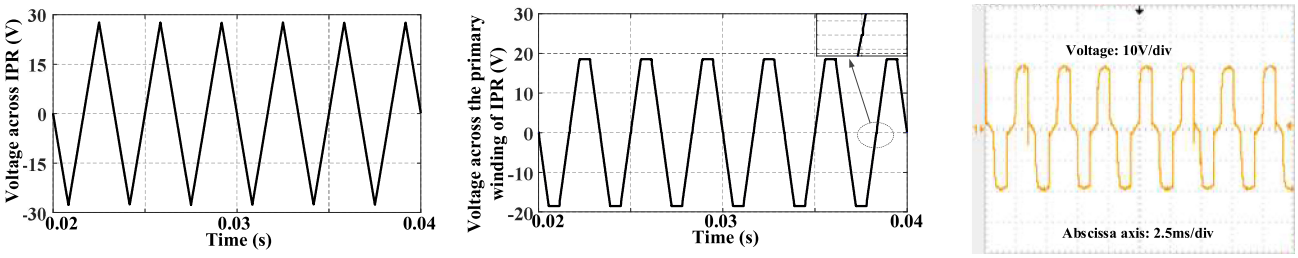

Fig. 12. Voltage across the primary winding of the multiwinding IPR. (a) Simulation result of the 12-pulse rectifier. (b) Simulation result of the proposed multipulse rectifier. (c) Experimental result of the proposed multipulse rectifier.

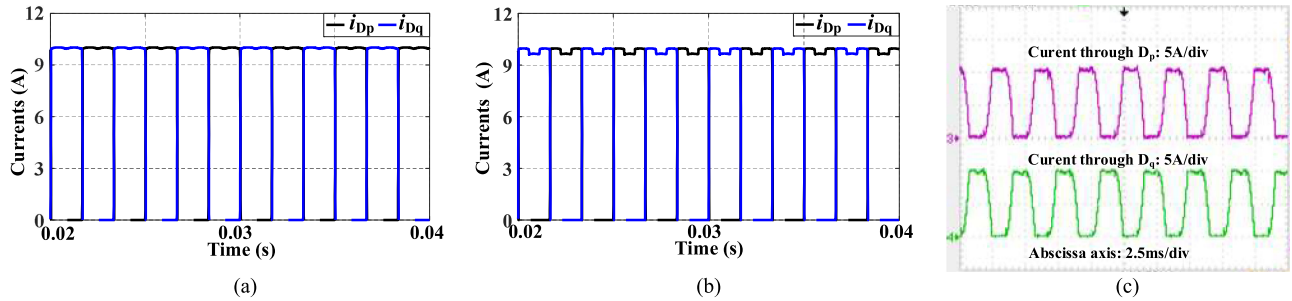

Fig. 13. Currents through the two diodes of the double-tapped IPR. (a) Simulation result of the 24-pulse rectifier. (b) Simulation result of the proposed multipulse rectifier. (c) Experimental result of the proposed multipulse rectifier.

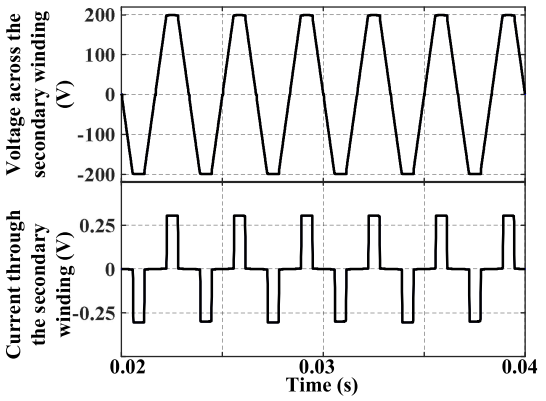

(a)

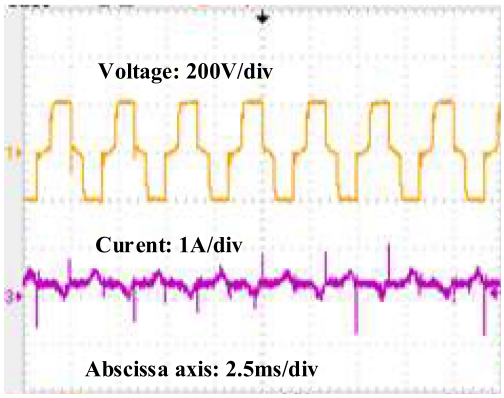

(b)

Fig. 14. Voltage across and current through the secondary winding of the multiwinding IPR. (a) Simulation results. (b) Experimental results.

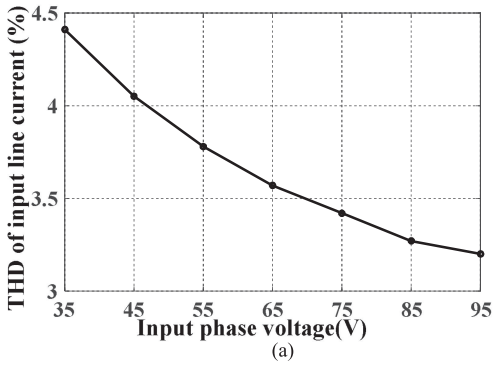

(a)

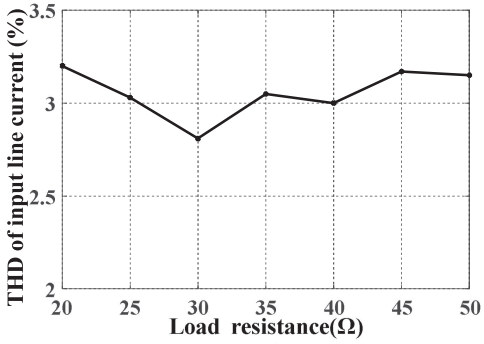

(b)

Fig. 15. The THD of the input line current. (a) When the load resistance is changed. (b) When the input phase voltage is changed.

and experimental results in the proposed multipulse rectifier, respectively. In the 12-pulse rectifier, the output voltage contains standardized six pulses per power supply cycle, and the output current is approximately constant under large inductive load. However, due to the modulation effect of the dual passive harmonic reduction methods, in the proposed multipulse rectifier, the output current contains six six-step waves per power supply cycle, and its step number is greater than that of the 12-pulse rectifier; in addition, due to the effect of the single-phase diode-bridge rectifier, the output voltage has six protuberances at the trough per power supply cycle.

Fig. 12(a) shows the voltage across the IPR in the 12-pulse rectifier, and Fig. 12(b) and (c) shows the simulation and experimental results of the voltage across the primary winding of the multiwinding IPR in the proposed multipulse rectifier, respectively. In the 12-pulse rectifier, the voltage across the IPR is approximately sixfold frequency triangular wave; in fact, in the 24-pulse rectifier using the double-tapped IPR, the voltage across the double-tapped IPR is also sixfold frequency triangular wave; however, due to the effect of the single-phase diode-bridge rectifier, the voltage across the primary winding of the multiwinding IPR contains six trapezoidal waves per power supply cycle.

Fig. 13(a) shows the currents through the two diodes connected with the double-tapped IPR in the 24-pulse rectifier, and Fig. 13(b) and (c) shows the corresponding simulation and experimental results in the proposed multipulse rectifier, respectively. From Fig. 13, the two diodes conduct in turn, and in the proposed multipulse rectifier, the currents have six little hollows per power supply cycle.

Fig. 14 shows the voltage across and current through the secondary winding of the multiwinding IPR. Because the turn ratio of the multiwinding IPR is about equal to 10.75, the current through the secondary winding is very small.

In order to validate the adaptability of the proposed multipulse rectifier, the input line currents are tested when the input voltages and the load resistance are changed, respectively. Fig. 15(a) shows the THD of the input line currents when the input voltage varies from 35 V to 95 V, and Fig. 15(b) shows the THD when the load resistance varies from 20 Ω to 50 Ω. From Fig. 15(a), when the input voltage is close to the rated value, the THD is minimal. Therefore, the proposed multipulse rectifier is sensitive to the variation of input voltage. However, when the input voltage varies, the THD, as a whole, meets the requirement in most of applications. From Fig. 15(b), the THD is less than 3.5% when the load resistance varies. Therefore, the proposed multipulse rectifier is insensitive to the variation of load resistance.

V. Conclusion

This paper proposed dual passive harmonic reduction methods to simultaneously reduce the harmonics of the input line current and the ripple of the load voltage in the multipulse diode-bridge rectifier. The dual passive harmonic reduction methods are realized by a multiwinding IPR. The primary winding of the multiwinding IPR and two diodes constitute the first method,

and the secondary winding and a single-phase diode-bridge rectifier constitute the second method. When the multiwinding IPR is designed optimally, the load voltage contains 36 pulses with equal width per power supply cycle, and its ripple coefficient is about 1.88×10^{-3}; the input line current contains 36 steps with equal width per power supply cycle, and its theoretical THD is about 5.04%. Compared with other harmonic reduction methods used in 12-pusle rectifier, the proposed methods can simultaneously increase the pulse number of load voltage and step number of input line current from 12 to 36. In addition, because only the diodes are used in the dual passive harmonic reduction methods, the proposed 36-pulse rectifier can be realized in a simple and easy way.

REFERENCES

[1] J. Solanki, N. Fröhleke, J. Böcker, A. Averberg, and P. Wallmeier, "High-current variable-voltage rectifiers: State of the art topologies," *IET Power Electron.*, vol. 8, no. 6, pp. 1068–1080, 2015.

[2] B. Singh, S. Gairola, B. N. Singh, A. Chandra, and K. Al-Haddad, "Multipulse AC-DC converters for improving power quality: A review," *IEEE Trans. Power Electron.*, vol. 23, no. 1, pp. 260–281, Jan. 2008.

[3] Z. Damin, W. Shitao, Z. Fengwu, W. Lujun, and L. Zhengyu, "Predictive fast DSP-based current controller for a 12-pulse hybrid-mode thyristor rectifier," *IEEE Trans. Power Electron.*, vol. 28, no. 11, pp. 5263–5271, Nov. 2013.

[4] A. Baghramian, A. Cross, and A. Forsyth, "Interactions within heterogeneous systems of uncontrolled rectifiers for aircraft electrical power systems," *IET Electr. Syst. Transp.*, vol. 1, no. 1, pp. 49–60, 2015.

[5] L. C. G. de Freitas, M. G. Simoes, C. A. Canesin, and L. C. de Freitas, "Performance evaluation of a novel hybrid multipulse rectifier for utility interface of power electronic converters," *IEEE Trans. Ind. Electron.*, vol. 54, no. 6, pp. 3030–3041, Dec. 2007.

[6] B. Singh, V. Garg, and G. Bhuvaneswari, "A novel T-connected autotransformer-based 18-pulse AC-DC converter for harmonic mitigation in adjustable-speed induction-motor drives," *IEEE Trans. Ind. Electron.*, vol. 54, no. 5, pp. 2500–2511, Oct. 2007.

[7] T. Yang, S. Bozhko, and G. Asher, "Functional modeling of symmetrical multipulse autotransformer rectifier units for aerospace applications," *IEEE Trans. Power Electron.*, vol. 30, no. 9, pp. 4704–4713, Sep. 2015.

[8] F. Meng, L. Gao, S. Yang, and W. Yang, "Effect of phase-shift angle on a delta-connected autotransformer applied to a 12-pulse rectifier," *IEEE Trans. Ind. Electron.*, vol. 62, no. 8, pp. 4678–4690, Aug. 2015.

[9] M. M. Swamy, "An electronically isolated 12 pulse autotransformer rectification scheme to improve input power factor and lower harmonic distortion in variable frequency drives," *IEEE Trans. Ind. Appl.*, vol. 51, no. 5, pp. 3986–3994, Sep./Oct. 2015.

[10] S. Bai and S. M. Lukic, "New method to achieve AC harmonic elimination and energy storage integration for 12-pulse diode rectifiers," *IEEE Trans. Ind. Electron.*, vol. 60, no. 7, pp. 2547–2554, Jun. 2013.

[11] F. Meng, W. Yang, S. Yang, and L. Gao, "Active harmonic reduction for 12-pulse diode bridge rectifier at dc side with two-stage auxiliary circuit," *IEEE Trans. Ind. Inform.*, vol. 11, no. 1, pp. 64–73, Feb. 2015.

[12] S. Choi, P. N. Enjeti, H. H. Lee, and I. J. Pitel, "A new active interphase reactor for 12-pulse rectifiers provides clean power utility interface," *IEEE Trans. Ind., Appl.*, vol. 32, no. 6, pp. 1304–1311, Nov./Dec. 1996.

[13] C.-M. Young, M.-H. Chen, C.-H. Lai, and D.-C. Shih, "A novel active interphase transformer scheme to achieve three-phase line current balance for 24-pulse converter," *IEEE Trans. Power Electron.*, vol. 27, no. 4, pp. 1719–1731, Apr. 2012.

[14] C.-M. Young, S.-F. Wu, W.-S. Yeh, and C.-W. Yeh, "A DC-side current injection method for improving ac line condition applied in the 18-pulse converter system," *IEEE Trans. Power Electron.*, vol. 29, no. 1, pp. 99–109, Jan. 2014.

[15] B. S. Lee, J. Hahn, P. N. Enjeti, and I. J. Pitel, "A robust three-phase active power-factor-correction and harmonic reduction scheme for high power," *IEEE Trans. Ind. Electron.*, vol. 46, no. 3, pp. 483–494, Jun. 1999.

[16] R. Abdollahi and G. B. Gharehpetian, "Inclusive Design and Implementation of Novel 40-Pulse AC-DC converter for retrofit application and harmonic mitigation," *IEEE Trans. Ind. Electron.*, vol. 63, no. 2, pp. 667–677, Feb. 2016.

[17] Q. Pan, W. Ma, D. Liu, Z. Zhao, and J. Meng, "A new critical formula and mathematical model of double-tap interphase reactor in a six-phase tap-changer diode rectifier," *IEEE Trans. Ind. Electron.*, vol. 54, no. 1, pp. 479–485, Feb. 2007.

[18] S. Choi, B. S. Lee, and P. N. Enjeti, "New 24-pulse diode rectifier systems for utility interface of high power AC motor drives," *IEEE Trans. Ind. Appl.*, vol. 33, no. 2, pp. 531–541, Mar./Apr. 1997.

[19] S. Miyairi, S. Iida, K. Nakata, and S. Masukawa, "New method for reducing harmonics involved in input and output of rectifier with interphase transformer," *IEEE Trans. Ind. Appl.*, vol. 22, no. 5, pp. 790–797, Sep./Oct. 1986.

[20] M. Fangang, Y. Shiyan, and Y. Wei, "Modeling for a multitap interphase reactor in a multipulse diode bridge rectifier," *IEEE Trans. Power Electron.*, vol. 24, no. 9, pp. 2171–2177, Sep. 2009.

[21] J. Arrillaga and M. Villablanca, "A modified parallel HVDC converter24 pulse operation," *IEEE Trans. Power Deli.*, vol. 15, no. 2, pp. 231–237, Apr. 2000.

[22] M. E. Villablanca and J. Arrillaga, "Pulse multiplication in parallel convertors by multitap control of interphase reactor," in *Proc. IEE -B: Electric Power Appl.*, Jan. 1992, vol. 139, no. 1, pp. 13–20.

[23] M. Fangang, G. Lei, Y. Wei, and Y. Shiyan, "Comprehensive comparison of the delta- and wye-connected autotransformer applied to 12-pulse rectifier," *J. Modern Power Syst. Clean Energy*, vol. 4, no. 1, pp. 135–145, Jan. 2016.

Lei Gao was born in Hebei, China, in 1982. She received the B.S., M.S., and Ph.D degrees in electrical engineering from the Harbin Institute of Technology, Harbin, China, in 2005, 2007, and 2012, respectively.

Since 2012, she has been a Lecturer with the Harbin Institute of Technology. Her current research interests include power electronics and motor drives.

Xiaona Xu was born in Shandong, China, in 1993. She received the B.S. degree in electrical engineering and automation, in 2016, from the Harbin Institute of Technology, Harbin, China, where she is currently working toward the M.S. degree in electrical engineering about power electronics and power drives.

Her research interests include multipulse rectifier, harmonic detection and reduction, and high-power rectification.

Zhongcheng Man was born in Shandong, China, in 1993. He received the B.S degree in electrical engineering in 2017 from the China University of Mining and Technology, Xuzhou, China. Since 2017, he has been working toward the M.S. degree in power electronics and power drives with Harbin Institute of Technology, Weihai, China.

His research interests include multipulse rectifier, power electronic transformer, and high-power rectification.

Junyuan Lee was born in Hubei, China, in 1975. He received the Ph.D. degree in electrical engineering, in 2006, from the Harbin Institute of Technology, Harbin, China. Since 2006, he has been working in power electronics and power drives with the Harbin Institute of Technology, Weihai, China.

His research interests include multipulse rectifier, power electronic transformer, and high-power rectification.